Science Advances

AAAS

advances.sciencemag.org/cgi/content/full/3/6/e1700685/DC1

Supplementary Materials for

Nanotwinned metal MEMS films with unprecedented strength and stability

Gi-Dong Sim, Jessica A. Krogstad, K. Madhav Reddy, Kelvin Y. Xie, Gianna M. Valentino, Timothy P. Weihs, Kevin J. Hemker

Published 28 June 2017, *Sci. Adv.* **3**, e1700685 (2017)
DOI: 10.1126/sciadv.1700685

This PDF file includes:

Supplementary Materials and Methods

Tensile specimens were pulled at room temperature using a custom-designed microtensile load frame consisting of a micro actuator, 25 lb load cell, air bearing and a Pixelink digital camera. The nominal strain rate during testing was 2×10^{-5} s^{-1}. Images of the gauge section were taken every 1 second to capture the surface image of the sample during loading. These images were post-processed using digital image correlation (DIC) technique to accurately measure the strain in the gauge length during loading. Instrumented nanoindentation was performed to measure hardness of the film at different strain rates using an iNano (Nanomechanics inc.) with a diamond Berkovich tip. The Oliver-Pharr method (*42*) was used to extract hardness from the nanoindentation load-displacement curves. All indentations were performed at constant indentation strain rates defined as

$$\dot{\varepsilon} = \frac{1}{h}\frac{\partial h}{\partial t} = \frac{1}{2}\left(\frac{1}{P}\right)\frac{\partial P}{\partial t} \quad \text{(S1)}$$

where h is indentation depth, t is time, and P is the applied load. Hardness data presented in Table 1 is the average of over 36 indentations at each strain rate.

Supplementary Text

Elastic modulus measurements

For a <111> textured fcc thin film, the elastic modulus E (111) is isotropic within the film plane and can be calculated from the single-crystal elastic constants using

$$E(111) = \frac{4}{2s_{11}+2s_{12}+s_{44}} = \frac{4}{2(0.00734)+2(-0.00274)+0.00802} = 232\ GPa \quad \text{(S2)}$$

where s_{ij} represents the compliance constants. This value of 232 GPa is based on single crystal elastic constants of bulk Ni (*43*), and the addition of Mo and W has been predicted to cause a slight increase in modulus (*8, 44*). However, the elastic modulus derived from the uniaxial tensile tests performed in this study is 221 GPa, which is 5% lower than the bulk value. Decreased elastic moduli for vapor-deposited metals have been reported by other authors (*45-48*) and attributed to a variety of factors. TEM images of the sputtered films rule out the influence of micro-cracks in the present study. The 5% decrease is likely related to minor variations in thickness or crystallographic texture.

Activation volume measurements

The activation volume Ω^* was calculated from the rate sensitivity of hardness using Eq. S3 and can be used to characterize thermally activated deformation processes. (*8, 49*)

$$\Omega^* = 3\sqrt{3}k_B T \frac{\partial ln\dot{\varepsilon}}{\partial H} \quad \text{(S3)}$$

where k_B is the Boltzmann constant, T is the temperature, $\dot{\varepsilon}$ is strain rate, and H is the hardness of the film. The activation volume of coarse grained polycrystalline FCC metals is ~1,000 b^3

(where the magnitude of the Burgers vector b = 0.25nm for Ni) and less than 20 b^3 when nanocrystalline and nanotwinned (*24*). Activation volumes for the $Ni_{83.6}Mo_{14}W_{2.4}$ films was measured to be below 20 b^3 (Table 1), which is consistent with nanotwins governed deformation.

Strengthening Mechanisms

The microstructure of the as-deposited films, single-phase solid solution alloy with a strong {111} texture and an ultra-high density of finely spaced nanotwins, led us to consider both solid solution strengthening and twin boundary strengthening.

The strengthening increment caused by local dislocation-solute interactions is (*20*)

$$\Delta\sigma_{Fleischer} = M \cdot \Delta\tau_{Fleischer} = M \cdot A \cdot G_{solvent} \cdot \varepsilon_S^{3/2} \cdot c^{1/2} \quad \text{(S4)}$$

where M is the Taylor factor (3.67 (*50*) assuming a perfect (111) textured polycrystalline film), A is a fitting constant (0.0235), G is the shear modulus (76 GPa), and c is the atomic fraction of the solute. ε_S represents the interaction parameter that accounts for the local resistance to dislocation propagation coming from changes in the lattice parameter and shear modulus in the vicinity of a solute atom

$$\varepsilon_S = \left| \frac{\frac{1}{G_{solvent}}\frac{\partial G}{\partial c}}{1+\frac{1}{2}\left|\frac{1}{G_{solvent}}\frac{\partial G}{\partial c}\right|} - 3\frac{1}{b_{solvent}}\frac{\partial b}{\partial c} \right| \quad \text{(S5)}$$

Substituting known values for Ni from the literature (*8, 51, 52*) gives a strengthening increment of 593 MPa.

The widely employed Hall-Petch relationship (*53, 54*) predicts the yield strength of a material when dislocations pile-up against grain boundaries. Here, instead of piling up at twin boundaries

the dislocations are expected to bow between twins in a manner similar to threading dislocations observed in thin films and multilayered materials (*21, 22, 55*). In this scenario, the strength increase originating from nanotwins can be predicted from the confined layer slip (CLS) model (*22*)

$$\Delta\sigma_{Nanotwins} = \sigma_0 + \beta\frac{Gb}{\lambda}\ln\left(\frac{\alpha\lambda}{b}\right) \quad \text{(S6)}$$

where σ_0 is lattice friction stress (37 MPa (*56*)), λ is the twin thickness, and α, β are material constants. Since α, β for nano-twinned Ni has not been reported, we used the value reported for Ti/Ni multilayer thin films ($\alpha = 0.16, \beta = 0.37$ (*57*)). It is worth considering how Eq. (S6) would be further affected by the presence of solutes. Similar to the analysis by Rupert et al. (*8*), solid solution additions are expected to affect the strength by changing the lattice parameter and shear modulus of the solvent, without change in the deformation mechanism. Strengthening increment from solid solution addition can be calculated as

$$\Delta\sigma_{Nanotwins,SS} \approx \beta\frac{Gb}{\lambda}\ln\left(\frac{\alpha\lambda}{b}\right)\cdot\left(\frac{1}{G_{solvent}}\frac{\partial G}{\partial c} + \frac{1}{b_{solvent}}\frac{\partial b}{\partial c}\right)\cdot c \quad \text{(S7)}$$

when higher order terms are neglected. The log term in Eqs. (S6) and (S7) becomes negative if the twin spacing is less than 4 nm, which is the case for our films. In order to predict the CLS stress for average twin spacing of 1.8 nm, CSL stresses calculated at larger twin spacing are extrapolated (using exponential curve fitting) to smaller twin spacing (fig. S2) (*22*).

These mechanisms are expected to operate in parallel, and the total strength of the nanotwinned solid solution films can be approximated by summing the influence of each mechanism. The total yield strength is then predicted to be:

$$\sigma_{YS,\ film} = \Delta\sigma_{\ Fleischer} + \Delta\sigma_{\ Nanotwins} + \Delta\sigma_{\ Nanotwins,SS} = 593 + 1{,}972 + 300 = 2{,}865\ \text{MPa} \qquad \text{(S8)}$$

which is close to the measured tensile strengths (Fig. 3 and Table 1). The agreement of the model with the experimental results, suggests that the model may be used to establish the potency of the various strengthening mechanisms, and the presence of the nanotwin structure clearly has the greatest effect.

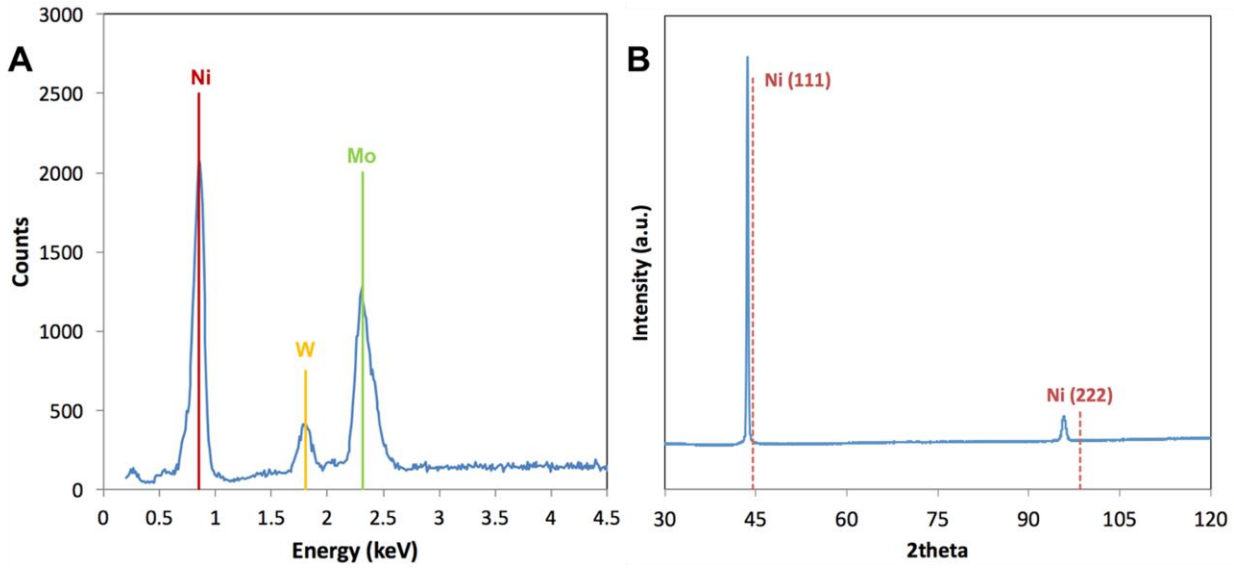

fig. S1. Scanning electron microscopy–EDS and XRD graph of the Ni-Mo-W film. (**A**) SEM-EDS graph of the as-deposited Ni-Mo-W film; (**B**) XRD result showing a strong (111) out-of-plane texture for the as-deposited Ni-Mo-W film.

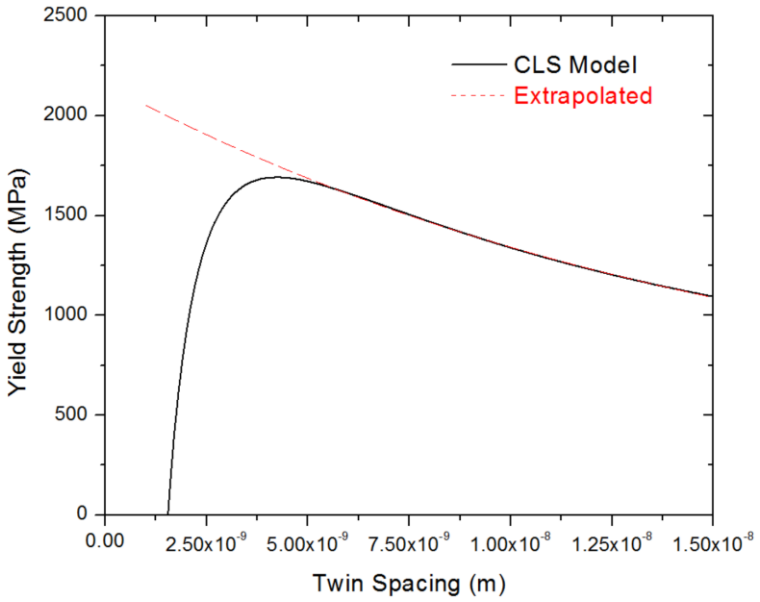

fig. S2. Yield strength predicted from the CLS model. In order to predict the yield strength of the as-deposited film, the CLS curve from larger twin spacing (> 4nm) is extrapolated to a smaller twin spacing. Extrapolation of the CLS model has been used to predict the yield strength of multilayer thin films with layer spacing ~1nm, but it may overestimate the yield strength if interface cutting by single dislocations occurs (*22*).